Effects of an epitaxial graphene layer for the growth of nickel silicides on a Ni(111) substrate

Fabio Ronci, Stefano Colonna, Roberto Flammini, Maurizio de Crescenzi, Manuela Scarselli, Matteo Salvato, Isabelle Berbezier, Holger Vach, Paola Castrucci

Effects of an epitaxial graphene layer for the growth of nickel silicides on a Ni(111) substrate

Fabio Ronci, Stefano Colonna, Roberto Flammini, Maurizio De Crescenzi, Manuela Scarselli, Matteo Salvato, Isabelle Berbezier, Holger Vach, Paola Castrucci

PII: S0169-4332(22)03291-3

DOI: https://doi.org/10.1016/j.apsusc.2022.155763

Reference: APSUSC 155763

To appear in: *Applied Surface Science*

Received date: 18 September 2022

Revised date: 7 November 2022

Accepted date: 16 November 2022

Please cite this article as: F. Ronci, S. Colonna, R. Flammini, et al., Effects of an epitaxial graphene layer for the growth of nickel silicides on a Ni(111) substrate, *Applied Surface Science* (2022), https://doi.org/10.1016/j.apsusc.2022.155763

Effects of an epitaxial graphene layer for the growth of nickel silicides on a Ni(111) substrate

Fabio Ronci [a,*], Stefano Colonna [a], Roberto Flammini [a], Maurizio De Crescenzi [b], Manuela Scarselli [b], Matteo Salvato [b], Isabelle Berbezier [c], Holger Vach [d], Paola Castrucci [b]
[a] Istituto di Struttura della Materia, CNR (ISM-CNR), 00133 Roma, Italy
[b] Dipartimento di Fisica, Università degli Studi di Roma "Tor Vergata", 00133 Roma, Italy
[c] CNRS, Aix-Marseille Universitè, IM2NP, UMR 7334, Campus de St. Jerome, 13397 Marseille, France
[d] LPICM, CNRS, Ecole Polytechnique, IPParis, 91128 Palaiseau, France
[*] Corresponding author. Email: ronci@ism.cnr.it

Abstract

In this paper, we report on an in-depth study on the growth of nickel silicides, either on a clean Ni(111) substrate or in the presence of a previously-grown epitaxial single graphene (Gr) layer, by means of Auger electron spectroscopy (AES), low energy electron diffraction (LEED), and scanning tunneling microscopy (STM). We demonstrate that two different nickel silicides, namely Ni_3Si and Ni_2Si, progressively form as the annealing temperature is increased from 450°C to 600°C. The presence of the Gr layer does not change the nature of the two silicide phases but rather affects the morphology of the silicide overlayer. Indeed, in the presence of Gr, the deposited silicon atoms intercalate by passing through the Gr defects or domain boundaries and accumulate on specific sample areas, resulting in the formation of multilayer silicide islands. In the absence of Gr, the deposited silicon atoms react uniformly with the nickel substrate, resulting in the formation of homogeneous large scale silicide layers.

Keywords

Graphene, Nickel, Nickel silicide, Auger electron spectroscopy, low energy electron diffraction, scanning tunneling microscopy

1. Introduction

The growth of thin-film nickel silicide crystals has been extensively studied over the last decades for their potential use in many applications including microelectronics and nanoelectronics [1-5], photovoltaics [6], and thin film coatings [7]. In this scenario, among the many ordered compounds (i.e. Ni_3Si, $Ni_{31}Si_{12}$, Ni_2Si, Ni_3Si_2, NiSi, and $NiSi_2$) exhibited by the Ni-Si binary phase diagram [8], the synthesis of thin films of Si-rich alloys has been thoroughly investigated during the annealing process of Ni depositions on Si substrates [9-13]. Conversely, Ni-rich compounds have been less studied and there are still open questions regarding the structure and reaction of silicidation with the Ni

substrate [14-16] and the possible formation of NiSi, an interesting low resistivity and low Si consumption material [17]. Recently, Vilkov et al. showed that it is possible to obtain graphene-capped nickel silicides by Si deposition on top of an epitaxial graphene layer grown on Ni(111) followed by annealing [18]. In particular, the authors report that several ordered nickel silicide phases (Ni_3Si, $Ni_{31}Si_{12}$, Ni_2Si, and NiSi) are progressively formed upon deposition of increasing amounts of Si on graphene-covered Ni(111) with subsequent annealing at 430°C.

In the present work, we report on the growth of nickel silicides, both with and without the graphene layer, on a Ni metal substrate, (111) oriented face. By depositing 1 monolayer (ML) of Si atoms at room temperature we followed the morphological and chemical changes occurring upon sample annealing by means of Auger electron spectroscopy (AES), low energy electron diffraction (LEED), and scanning tunneling microscopy (STM). Our results show that, regardless of the presence of the graphene layer, the same nickel silicide phases are formed upon progressive annealing and that its presence only affects the morphology of the resulting silicide domains. In particular, at first a 2x2 reconstruction is detected upon annealing at 450°C and attributed to the formation of Ni_3Si. By increasing the annealing temperature, the 2x2 reconstruction is gradually transformed into $(\sqrt{3}x\sqrt{3})R30°$, denoting the conversion of Ni_3Si to Ni_2Si. At 600°C the phase transition is completed, while at annealing temperature ≥ 700°C, the disappearance of any ordered phase and a (partial) Si dissolution in the bulk Ni is observed. As far as morphology is concerned, the Si/Ni(111) surface after annealing displays the formation of a reconstructed surface with single layer (about 0.2 nm thick) terraces, while the presence of the graphene layer produces the formation of multilayered islands, which extend their lateral size with increasing annealing temperature up to 600°C, though maintaining their apparent height. We attribute these morphology differences to the fact that without graphene Si atoms have all the Ni surface available to interact with, while in the presence of a graphene layer Si atoms can only intercalate through graphene defects and/or domain boundaries, thus locally interacting with the Ni atoms and favoring the formation of multilayer islands.

2. Experimental

Samples were prepared in an UHV preparation chamber with a base pressure below 1×10^{-10} mbar. A single crystal Ni(111) substrate was cleaned by Ar^+ sputtering (T = 950 K, E = 1.0-0.5 keV) and annealing (T= 1125 K). Single layer graphene was grown on the clean Ni(111) substrate according to the procedure described in Ref. [19]. Silicon deposition was performed either on the clean Ni(111)

sample or on the freshly-made Gr/Ni(111) substrate kept at room temperature (RT) using an electron bombardment source at constant flux rate of about 0.01 nm/min. Source calibration was achieved by using a refrigerated quartz crystal thickness monitor placed at the very same sample position before and after Si deposition [19]. Silicon coverage will be reported in terms of monolayers (ML), where 1ML corresponds to 1 Si atom per Ni(111) unit cell; i.e., to about 0.37 nm of Si equivalent thickness. In the experiments reported here, the deposition of Si was fixed to 1ML. LEED patterns and Auger spectra as a function of annealing were obtained using an Omicron Specta-LEED optics. After annealing, the samples were always cooled down to RT before measurement. The AES spectra were collected as first derivative of the electron yield. STM measurements were obtained using a Low Temperature STM Omicron (LT-STM) housed in a UHV chamber with a base pressure below 5×10^{-11} mbar, connected to the preparation chamber. The STM images were acquired at RT using a W tip cleaned by electron bombardment in UHV, after scanner calibration performed measuring the clean Ni(111) surface.

3. Results

3.1 Auger electron spectroscopy

In Fig. 1 we report the AES spectra recorded before and after Si deposition on both Ni(111) and Gr/Ni(111) samples kept at room temperature (RT). The presence of Gr, demonstrated by the C KVV peak at about 275 eV, results in a reduced intensity of the Ni $M_{2,3}VV$ peak in the Gr/Ni(111) spectrum (see Figs. 1(a) and 1(b) for comparison). On the other hand, the comparison of the spectra recorded after Si deposition in Figs. 1(c) and 1(d) reveals a significant width difference between the Si $L_{2,3}VV$ peaks of Si/Ni(111) and Si/Gr/Ni(111), with FWHM values of 7.3 eV and 4.4 eV, respectively. This result suggests a different reactivity of Si with the Ni(111) and the Gr/Ni(111) substrates. Indeed, in the Si/Ni(111) case, silicon atoms react with the nickel substrate at RT, forming a continuous layer of amorphous nickel silicide, as indicated by the large Si $L_{2,3}VV$ peak, an evidence that was already reported in the literature for RT deposition of both Si on Ni(111) [14] and Ni on Si(111) [12]. Conversely, in the case of Si deposition on the Gr/Ni(111) substrate at RT, Si remains mostly on top of the Gr layer forming silicon nanoparticles leaving most of the Gr surface uncovered [18], as demonstrated by the much narrower Si $L_{2,3}VV$ peak in Fig. 1(d) [20].

The second part of the study focused on the effect of a progressive annealing on both Si/Ni and Si/Gr/Ni samples. In Fig. 2 we report the peak-to-peak intensity of the Si $L_{2,3}VV$ and the C KVV peaks (normalized to the peak-to-peak intensity of the Ni $M_{2,3}VV$ peak) as a function of annealing

temperature. For the Si/Ni sample (red hollow circles), one can clearly see a gradual, almost linear intensity decrease, reaching a minimum limiting value of about 13% of the RT intensity between 700 and 800°C.

In the case of the Si/Gr/Ni(111) sample (red solid circles), a slope discontinuity is observed slightly below 400°C, temperature at which silicon is known to significantly intercalate below Gr [18]. At higher annealing temperatures the two samples show very similar behavior (the normalized Si signal remains well above zero), indicating that silicon does not completely diffuse into the nickel crystal bulk even at temperatures as high as 850°C. The normalized C KVV intensity (black solid squares) remains constant up to about 500°C, while a large decrease is observed between about 550 and 750°C, in agreement with the well-known C dissolution process into the Ni crystal occurring at about 650°C [21].

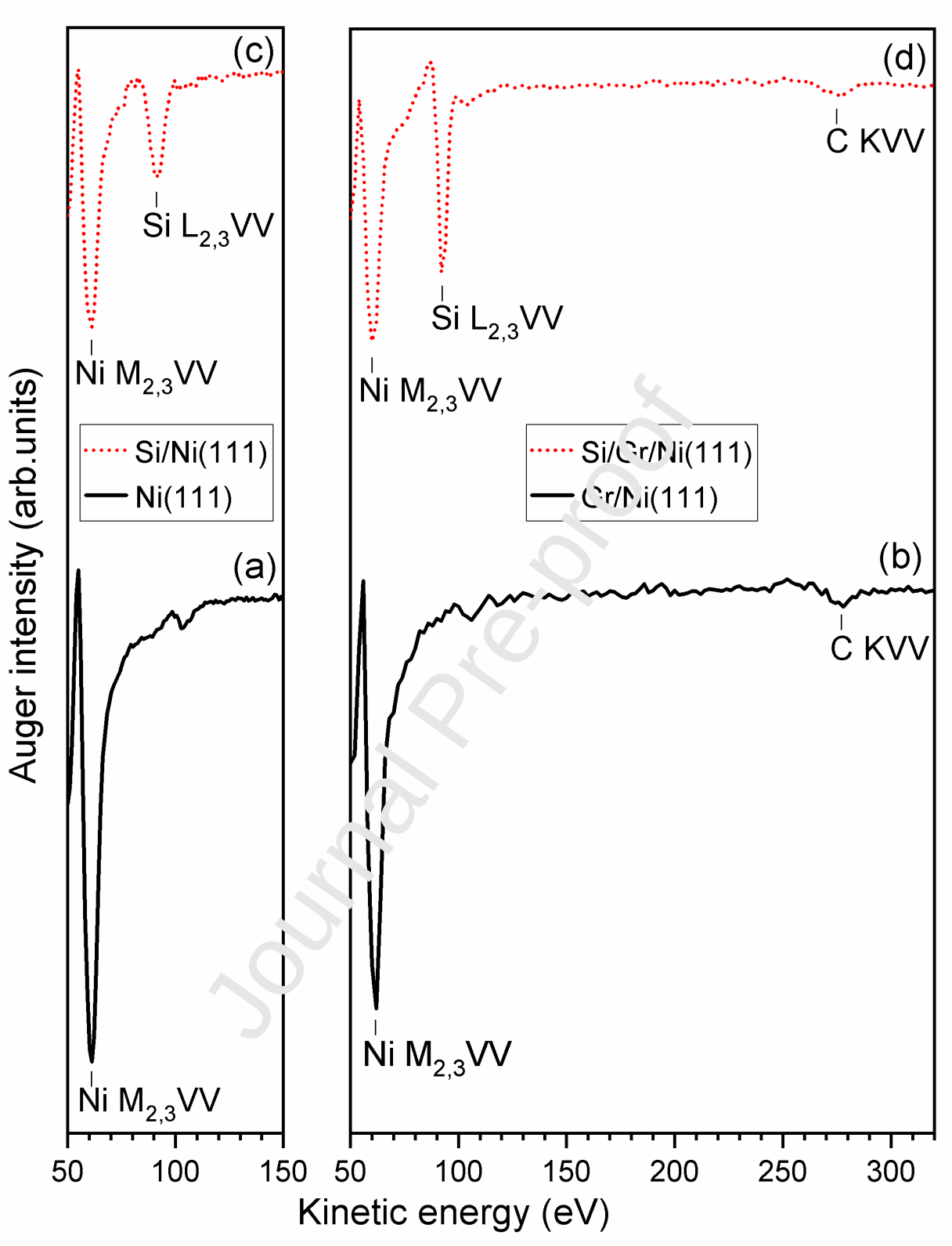

Figure 1 – Left: AES spectra of Ni(111) before (a) and after (c) Si deposition at RT. Right: AES spectra of Gr/Ni(111) before (b) and after (d) Si deposition at RT.

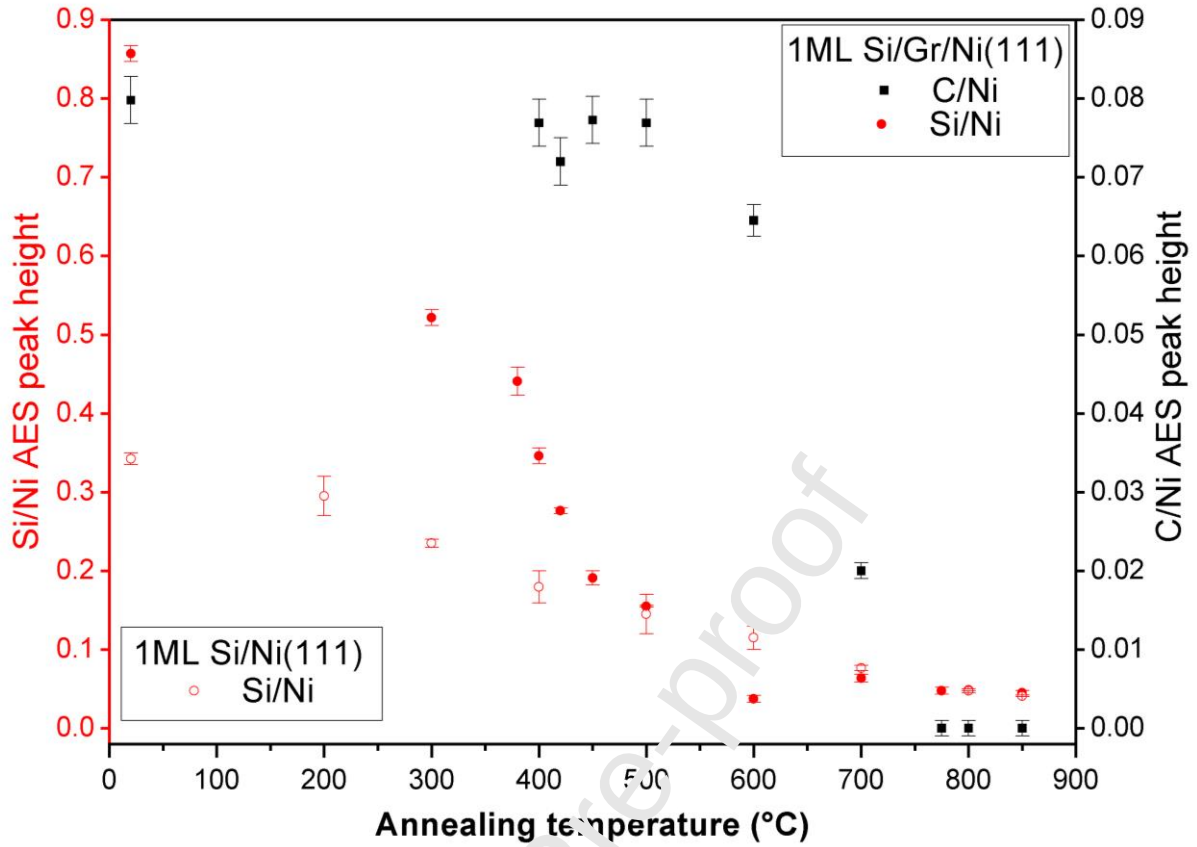

Figure 2 – Si $L_{2,3}VV$ and C KVV AES peak-to-peak intensities normalized to the peak-to-peak Ni $M_{2,3}VV$ intensity, as a function of annealing temperature. Left y axis (red circle symbols): Si $L_{2,3}VV$ AES peak-to-peak intensity of the Si/Gr/Ni(111) (solid symbols) and the Si/NI(111) (hollow symbols) samples. Right y axis (black symbols): C KVV AES peak-to-peak intensity of the Si/Gr/Ni(111) sample.

3.2 Low energy electron diffraction (LEED)

Along with Auger spectra, LEED patterns were acquired after Si deposition as a function of annealing temperature and reported in Fig. 3. The LEED patterns acquired before Si deposition on Ni(111) and on Gr/Ni(111) showed in both cases the sole presence of bulk Ni(111) spots, as already observed in Refs [19,22], given the quite small lattice mismatch that consents the epitaxial growth of Gr on Ni(111). We emphasize the absence of streaks in the Gr/Ni(111) LEED pattern, excluding the presence of rotated Gr domains, as reported in Ref. [21].

Si deposition at RT on Ni(111) results in the complete disappearance of the substrate bulk spots, showing a strong diffuse background (panel a). On the contrary, after Si deposition on Gr/Ni(111), see panel b), faint bulk spots of the Ni(111) substrate (and of the epitaxial Gr layer) are still visible and a weaker background is observed.

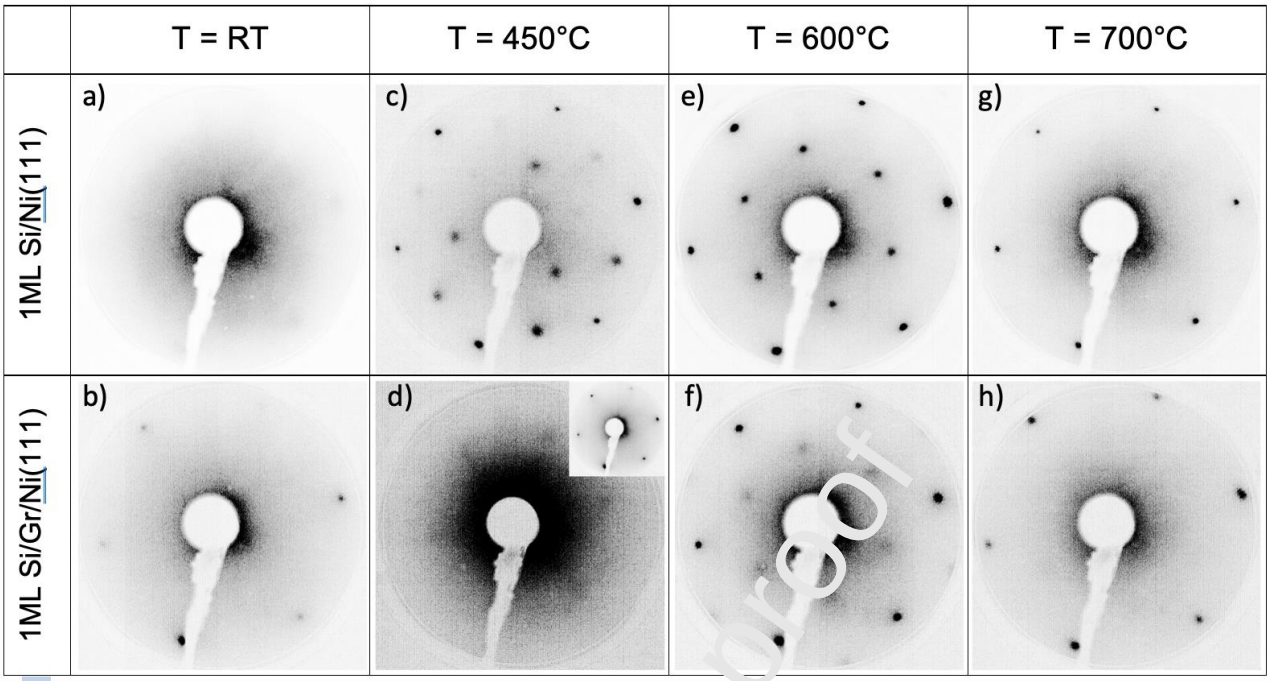

Figure 3 – LEED patterns recorded after Si deposition at RT on Ni(111) and Gr/Ni(111) (left and right columns, respectively) as a function of annealing temperature. All patterns were obtained at 80 eV electron beam energy except the one in panel d, recorded at 45 eV beam energy (inset at 80eV). See text for discussion.

A progressive annealing of the Si/Ni(111) sample up to 450°C results in a strong reduction of the diffuse background and the appearance of a 2x2 reconstruction (panel c), indicating the formation of an ordered nickel silicide phase out of the amorphous one. The nature of such a phase will be discussed afterwards.

As for the Si/Gr/Ni(111) sample, the annealing procedure leads to the formation of a similar, but very faint, 2x2 modulation, which is visible only at 45eV (panel d) but not at 80eV (inset), suggesting the formation of the same phase. A further temperature increase to 600°C in both cases leads to a gradual phase transition from 2x2 to ($\sqrt{3}$x$\sqrt{3}$)R30°,(panels e and f). During the annealing procedure of the Si/Ni(111) sample, the LEED pattern (not reported) shows the concomitant presence of both 2x2 and ($\sqrt{3}$x$\sqrt{3}$)R30° spots, indicating the coexistence of the two phases at intermediate temperatures.

Finally, after annealing at 700°C, only the substrate bulk spots are visible in the LEED patterns of both systems. Indeed, the AES results in Fig. 2 show a significant reduction of both C and Si

intensities at such a temperature, indicating that the larger part of surface C and Si dissolved in the Ni Bulk resulting in the disappearance of any surface reconstruction.

3.3 Scanning tunneling microscopy (STM)

In Fig. 4 we report in panels (a) and (b) the STM images of the two samples after Si deposition at RT and the relative line profiles in panel (g). Such images show the formation of a disordered layer covering the whole substrate in the case of Si deposition on Ni(111), while Si clustering is observed for Si deposition on Gr/Ni(111).

After annealing at 450°C, temperature at which a 2x2 reconstruction appears in the LEED patterns, flat islands are observed in both cases. It must be noticed that mainly single layer islands are formed on the Si/Ni(111) sample, as indicated by their 0.2 nm apparent step height, while the growth of multilayer islands is observed on Si/Gr/Ni(111), as evident by comparing Fig. 4 (c)-(d) and the relative line profiles in Fig. 4 (g).

Subsequent annealing at 600°C, causing a 2x2→(√3x√3)R30° phase transition according to LEED patterns, produces the almost complete disappearance of islands in the Si/Ni(111) sample, while larger multilayer islands, maintaining the same apparent step heights as measured at 450°C, are observed in the Si/Gr/Ni(111) one, see Figs. 4 (e) and (f) and line profiles in panel (i).

Atomic resolution STM images of the annealed Si/Ni(111) sample are reported in Fig. 5, along with line profiles, confirming the formation of single layer, 0.2 nm high islands, and the relative differentiated images to better highlight the atomic corrugation on both the island and the terrace. Despite the presence of atomic disorder, the STM images obtained after annealing at 450°C, reported in Figs. 5 (a) and (b), display a clear 2x2 reconstruction, as demonstrated by the comparison with the Ni(111) image in the inset, whose scale has been deliberately doubled with respect to the other images. Clearly, such a 2x2 reconstruction is present both on the island and on the underlying terrace. On the other hand, the STM images in Figs. 5 (c) and (d) clearly show an almost complete conversion to a (√3x√3)R30° reconstruction after annealing to 600°C, with a residual 2x2 phase still present in small sample areas. Such images are hence in good agreement with the LEED results, confirming a 2x2→(√3x√3)R30° phase transition occurring for annealing temperatures between 450 and 600°C.

Fig. 6 reports the STM images obtained after annealing the Si/Gr/Ni(111) sample at 450°C (a) and at 600°C (c). As already observed in Figs. 4 (d) and (f), in this case multilayer islands are formed, as evident by the typical line profiles that can be obtained on such islands, reported in Figs. 6 (e) and

(f). The atomic resolution of such images is emphasized by the differentiated images reported in (b) and (d). In both images a hexagonal lattice is clearly visible, compatible with the presence of a continuous Gr layer on top covering both the substrate and the island. Interestingly, extended defective areas, indicated by blue dotted ovals, are visible in the differentiated STM image in (b).

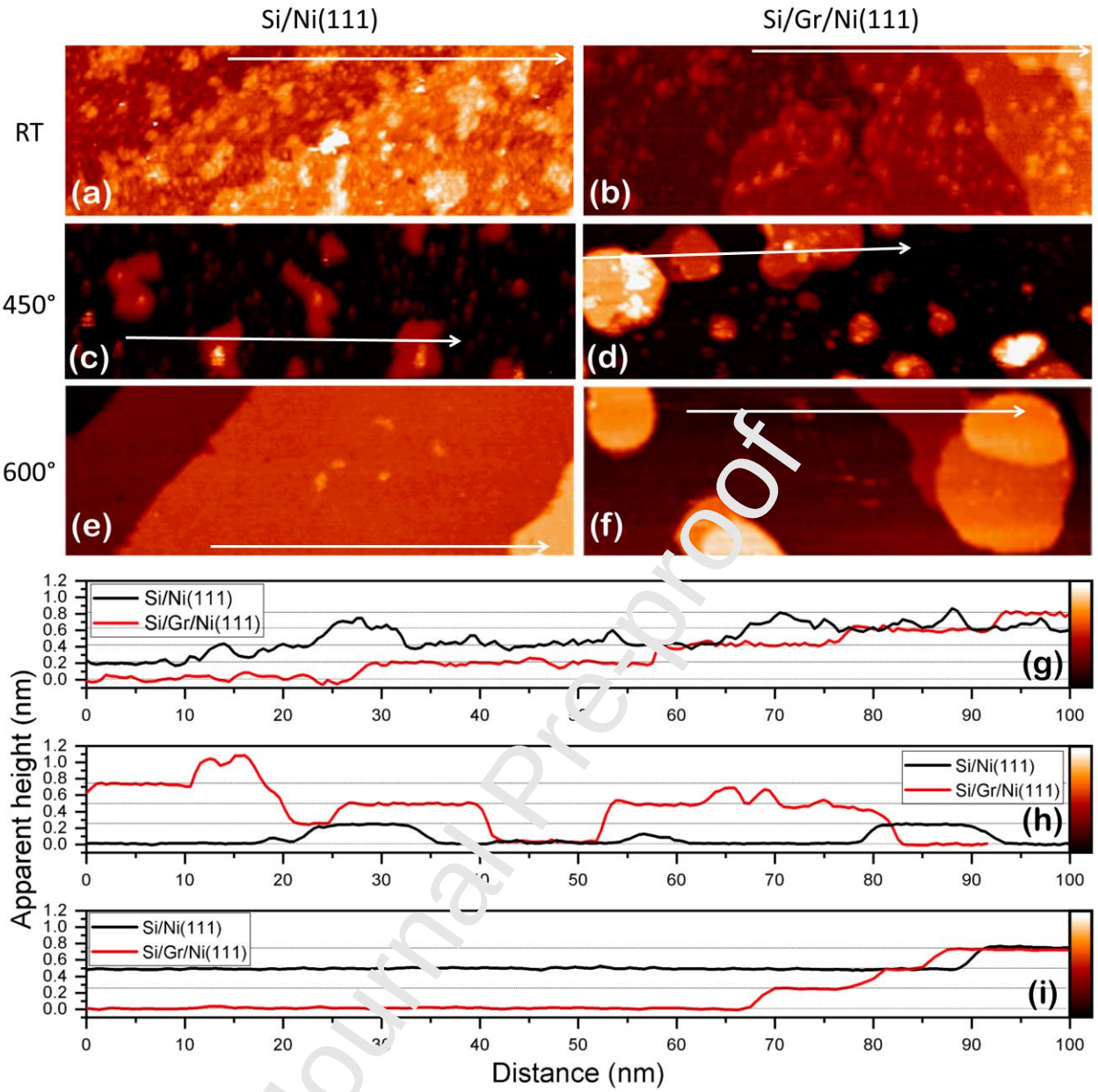

Figure 4 – (a-f): 150x50 nm² STM images obtained after 1ML Si deposition at RT on Ni(111) (left column) and on Gr/Ni(111) (right column). (a) (V_{sample} = -1 V, I = 5 nA) and (b) (V_{sample} = -0.01 V, I = 20 nA): before annealing. (c) (V_{sample} = -1 V, I = 5 nA) and (d) (V_{sample} = -0.05 V, I = 50 nA): after annealing at 450°C. (e) (V_{sample} = -0.05 V, I = 50 nA) and (f) (V_{sample} = -0.01 V, I = 50 nA): after further annealing at 600°C. (g): line profiles taken along the arrows in (a) and (b); (h): line profiles taken along the arrows in (c) and (d); (i): line profiles taken along the arrows in (e) and (f).

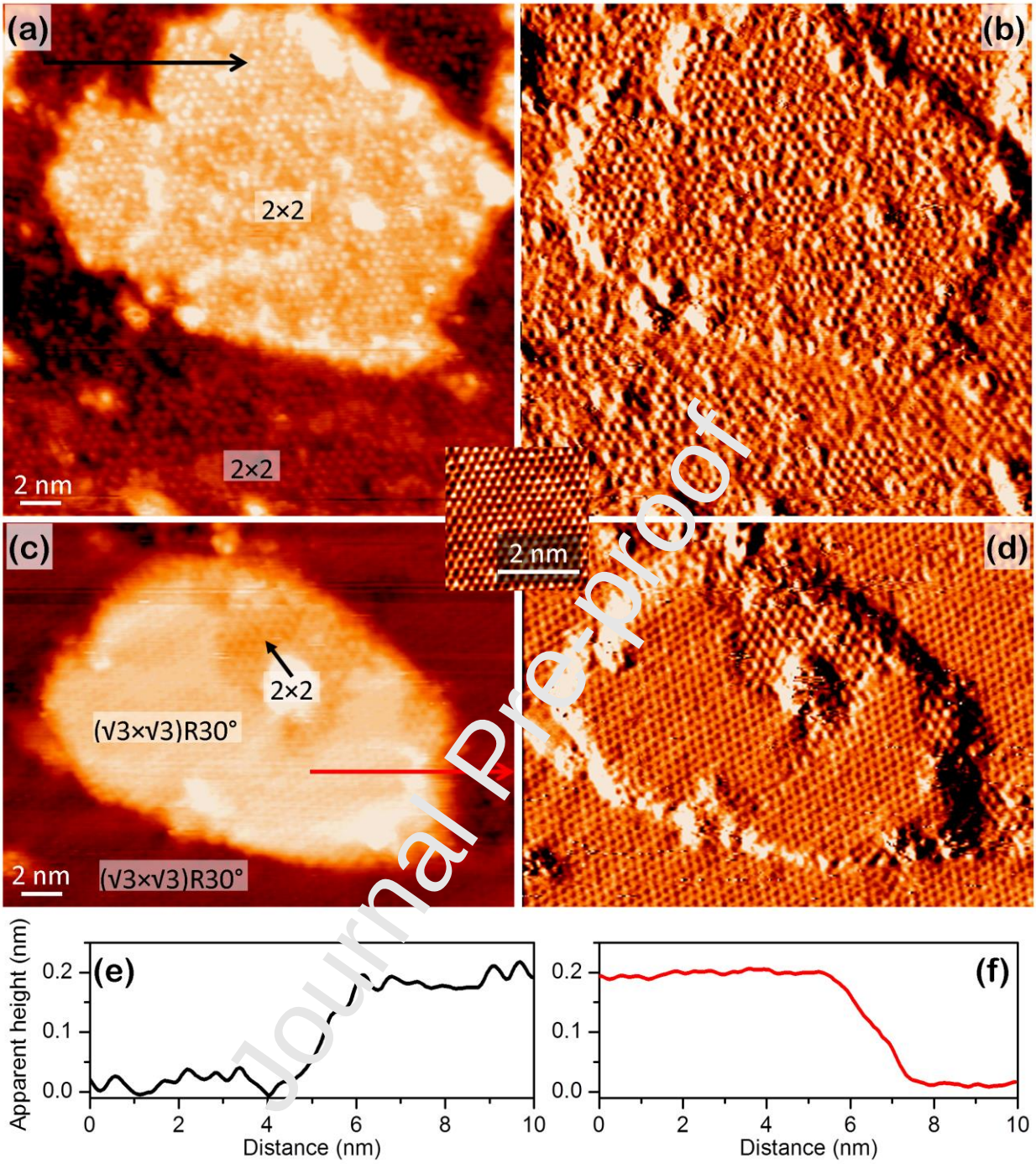

Figure 5 – (a): 25.0 x 25.0 nm^2 STM image (V_{sample} = -0.5 V, I = 5 nA) after 1ML Si deposition at RT on the Ni(111) sample and annealing at 450°C. (b): same image after differentiation along the x direction. (c): *25.0 x 18.75 nm^2 STM image (V_{sample} = -1.0 V, I = 5nA) after 1ML Si deposition at RT on the Ni(111)* sample and annealing at 600°C. (d): same image after differentiation along the x direction. *(e): line profile along the black arrow in (a). (f): line profile along the red arrow in (c).* A Ni(111) *3.5 x 3.5 nm^2* STM image *(V_{sample} = 0.01 V, I = 50 nA)* is reported in the inset with a doubled scale compared to the one of the other images for better visibility and better comparison with the *2x2 phase.*

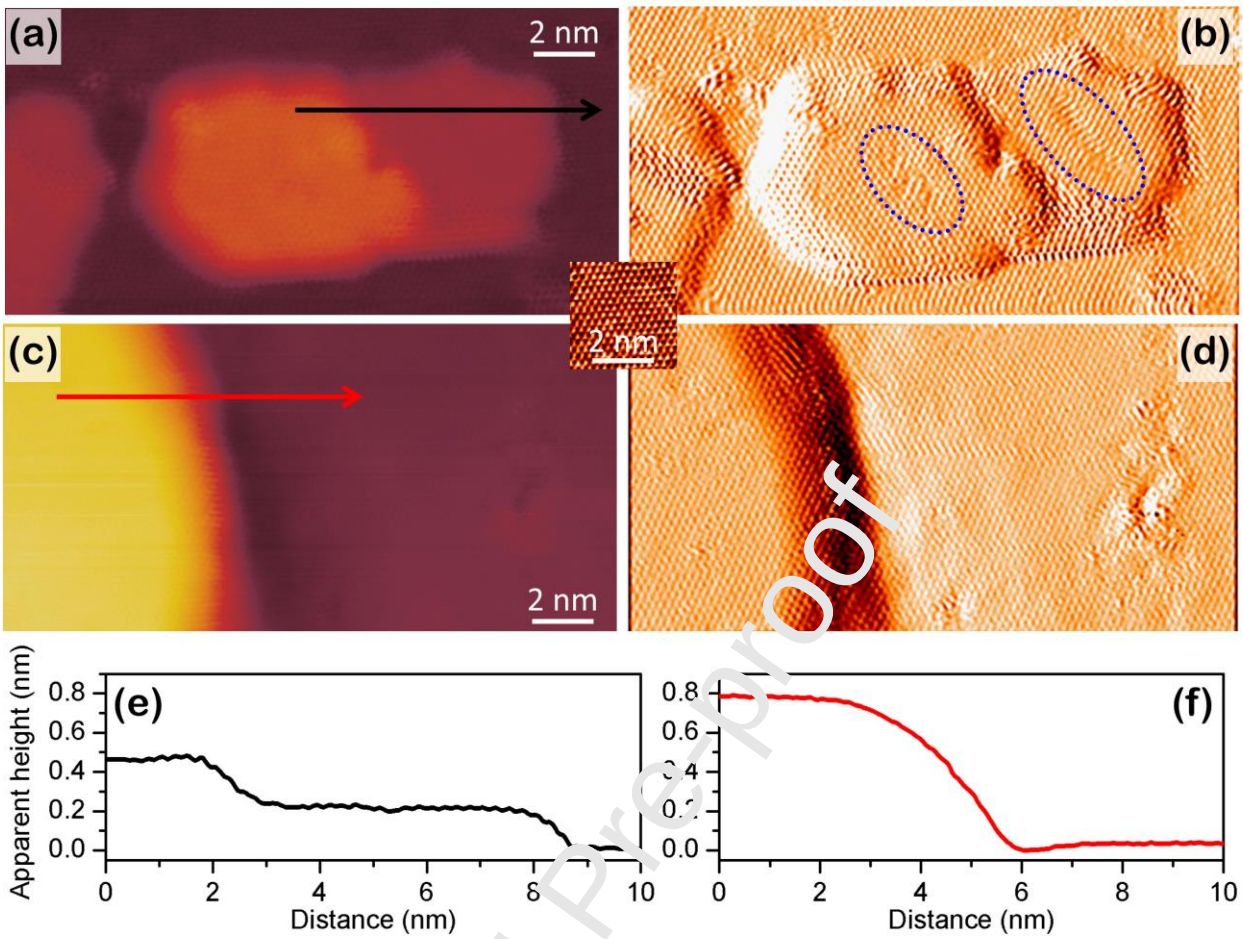

Figure 6 – (a): 20 x 10 nm² STM image (V_{sample} = +0.02 V, I = 50 nA) after 1ML Si deposition at RT on the Gr/Ni(111) sample and annealing at 450°C. (b): same image after differentiation along the x direction. (c): *20 x 10 nm² STM image (V_{sample} = -0.01 V, I = 100 nA) after 1ML Si deposition at RT on the Ni(111)* sample and annealing at 600°C . (d): same image after differentiation along the x direction. *(e): line profile along the black arrow in (a). (f): line profile along the red arrow in (c).* A Ni(111) *3.5 x 3.5 nm²* STM image *(V_{sample} = 0.01 V, I = 50 nA)* is reported in the inset.

4. Discussion

4.1 Si/Ni(111)

Both LEED and STM measurements taken at RT confirm the presence of an amorphous (or very small grain size polycrystalline) layer of nickel silicide, as already reported in the literature [14, 23]. Indeed, the almost complete disappearance of the Ni(111) bulk spots suggests a strong intermixing of Si with the topmost Ni layers [14].

Progressive annealing results in the appearance of novel reconstructions in the LEED patterns reported in Fig. 3. This suggests the formation of different crystalline nickel silicide phases resulting

from the ordering of the amorphous layer formed at RT. The bulk binary Si-Ni phase diagram is particularly rich and several silicides may form depending on temperature and relative Si-Ni amount: Ni_3Si, $Ni_{31}Si_{12}$, Ni_2Si, Ni_3Si_2, NiSi, and $NiSi_2$ [8].

According to the literature, deposition of tens of nm of Ni on a Si crystal at RT, followed by an annealing procedure, results in the progressive formation of Si-rich silicides, namely Ni_2Si, Ni_3Si_2, NiSi and $NiSi_2$. On the other hand, applying the same annealing procedure on tens of nm of Si deposited on a Ni crystal gives rise to the formation of silicides with increasing nickel content: Ni_2Si, $Ni_{31}Si_{12}$, and Ni_3Si [24-27]. In the above-discussed cases, the silicide formation is controlled primarily by the annealing temperature, given the large amount of deposited Si. Conversely, when monolayer or sub-monolayer quantities are deposited, the stoichiometry of the formed silicides can strongly depend on the amount of the deposited element and on the epitaxy relation between silicide and substrate. For example, Rahman et al. report the formation of Ni_2Si attested by a $(\sqrt{3}x\sqrt{3})R30°$ reconstruction after annealing at 850K (i.e. about 580°C) for 1/3 ML Si deposited on Ni(111). At higher coverage of about (0.56-0.84) ML, the formation of NiSi is indicated by a 2x2 reconstruction [15, 17]. Conversely, Lalmi et al. report the exclusive formation of Ni_2Si ($(\sqrt{3}x\sqrt{3})R30°$) for 1 ML Si deposition on Ni(111) in the 130-650°C temperature range [14].

In this work, the first phase transition detected by LEED is witnessed by the appearance of a 2x2 reconstruction at 450°C, Fig. 3 (c). Such a reconstruction, apparently overlooked in the same experimental conditions by Lalmi et al., may be the signature of the formation of either Ni_3Si or NiSi. Indeed, substituting ¼ of the Ni atoms in the first layer of the Ni(111) substrate with Si atoms, Fig. 7 (a), left model, results in a clear 2x2 surface reconstruction with a Ni_3Si stoichiometry.

On the other hand, NiSi is reported to form a 2x1 surface reconstruction [17] (Fig. 7 (a), right model) with 3 domains orientation along the high symmetry substrate directions, resulting in a 2x2 LEED pattern as well. The actual nature of the 2x2 reconstruction observed in the LEED pattern is unveiled by the STM image reported in Fig. 5(a-b), showing a clear 2x2 reconstruction all over on the sample surface, hence revealing the formation of Ni_3Si. Indeed, the STM images Fig. 5 (a-b) are representative of the whole sample: we never observed 2x1 domains that would have suggested the formation of NiSi.

In Fig. 7 (b-c) we report the ball model of the bulk truncated $Ni_3Si(111)$ hexagonal surface obtained from the cubic (space group Pm-3m) Ni_3Si crystal structure reported in the literature [28, 29]. The top view is identical to the one reported in the left model in Fig. 7 (a), obtained substituting one Ni atom out of four with a Si atom, except for a very small lattice mismatch of about 0.5%.

Furthermore, the measured island step height of about 0.2nm reported in Fig. 4 (c) fits well with the crystallographic value of 0.2045 nm reported in Fig. 7 (c).

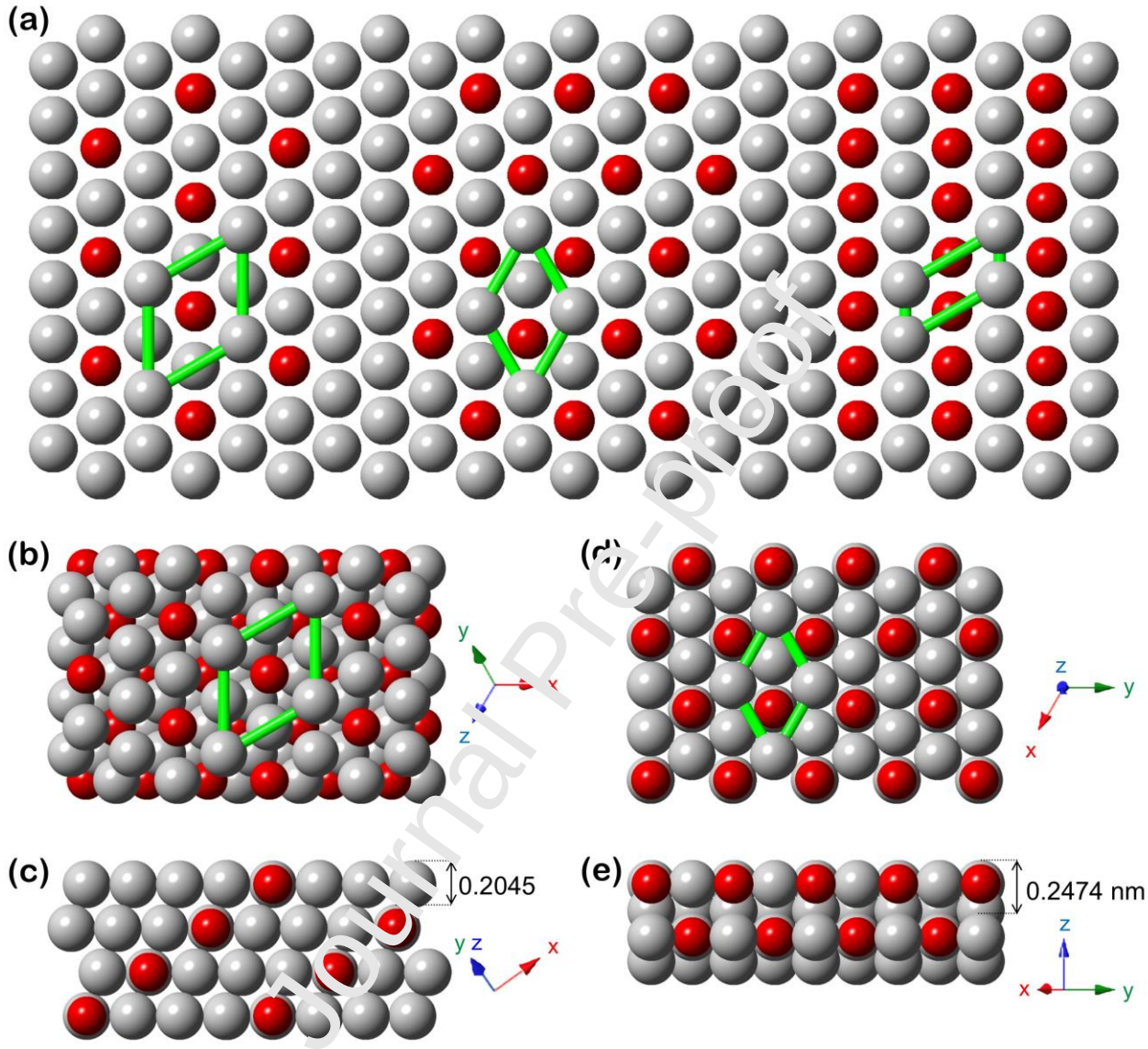

Figure 7 – (a): tentative ball models of Ni_3Si (*left*, 2x2 reconstruction), Ni_2Si (*center*, $(\sqrt{3}x\sqrt{3})R30°$ reconstruction) and NiSi (*right*, 2x1 reconstruction) ordered phases obtained by selective substitution of Ni (gray balls) with Si atoms (red balls) in a Ni(111) topmost layer, top view. *(b-e):* ball models of the bulk-truncated $Ni_3Si(111)$ (b-c) and of the $Ni_2Si(001)$ (d-e) surfaces. Top and side views are reported in the upper and lower panels, respectively.

Hence, we infer that the 2x2 reconstruction results from the formation of Ni_3Si rather than NiSi, in contradiction with Ref. [17]. We notice here, however, that in Ref. [17] the authors adopted a different deposition procedure, studying the phase transition as a function of Si coverage while keeping the Ni(111) sample at 850K. Following that procedure, they detected at first a (√3x√3)R30° reconstruction attributed to the formation of Ni_2Si and then a 2x2 phase, attributed to NiSi, keeping the Si coverage well below 1ML. Therefore, we suggest that the different Si coverages and different annealing procedures may be the cause of the different conclusions on the nature of the 2x2 phase. A second phase transition to a (√3x√3)R30° reconstruction is observed by LEED upon further increasing the annealing temperature. The maximum intensity of the novel reconstruction spots is observed at about 600°C, Fig. 3 (e). The formation of domains with (√3x√3)R30° reconstruction is confirmed by the STM image in Fig. 5 (c-d). In agreement with the literature results, we attribute this novel phase to Ni_2Si [14,15], whose (√3x√3)R30° reconstruction can be modeled substituting one surface Ni atom out of three with Si, see Fig. 7 (a), central model. In Fig. 7 (d-e) we report the ball model of the bulk truncated $Ni_2Si(001)$ surface according to the crystallographic data reported for its hexagonal (space group $P6_3/mmc$) bulk phase [30, 31]. The top view clearly resembles the bottom-right model in Fig. 7, though the unit cell parameter is about 11% larger than Ni(111). Besides, in this case, the side view clearly shows that a buckling is present in the bulk-truncated $Ni_2Si(111)$ surface, resulting in a larger step height value of 0.2474 nm. The epitaxial growth of such a phase on the Ni(111) surface is however expected to form structures with a reduced buckling and, as a consequence, with a reduced step height, possibly approaching the experimental value 0.2 nm. Finally, as the temperature is further increased, Si diffuses in the bulk, the (√3x√3)R30° reconstruction disappears, as observed by the LEED pattern in Fig. 3 (g), and the Si/Ni AES peak height ratio reaches its minimum value, see Fig. 2.

4.2 Si/Gr/Ni(111)

In comparison with the case of Si/Ni(111), after Si deposition on the Gr/Ni(111) substrate at RT, the LEED pattern in Fig. 3 (b) shows a lower background and the bulk 1x1 spots of Ni(111) and of the epitaxial graphene remain visible. Indeed, the corresponding STM image in Fig. 4 (b) shows the formation of Si clusters on top of the substrate, whose surface remains largely uncovered. A detailed study of this system has been reported elsewhere, showing that, in addition to Si clusters on top of the graphene layer, a small amount of Si is able to intercalate below the Gr layer forming bi-dimensional Si disordered islands [19].

Upon progressive annealing of the Si/Gr/Ni(111) sample between 400°C and 450°C, silicon intercalates below Gr [18], as testified by AES spectra Fig. 2. In concomitance, the LEED pattern recorded at 450°C shows very faint 2x2 spots. Comparing Figs. 3 (c) and 3 (d), we can observe that the same 2x2 reconstruction is obtained for both samples after annealing at 450°C, suggesting the formation in both cases of the same Ni_3Si phase. The same conclusion was drawn by Vilkov et al. [18], reporting the formation of a Ni_3Si silicide phase beneath the Gr layer with a clear 2x2 reconstruction upon deposition of 12 Å of Si and subsequent annealing at 500°C. In our case a lower dose (1ML, corresponding to about 3.7 Å) was deposited on top of the Gr/Ni(111) sample, justifying the much weaker intensity of the observed 2x2 LEED pattern. Furthermore, the STM images of the Si/Gr/Ni(111) sample after annealing at 450°C reported in Fig. 4 (d) show the formation of multilayer islands whose height is an integer multiple of about 0.2 nm, as shown by the line profile in Fig. 4 (g), in agreement with the step height values measured in absence of Gr.

The large scale STM image in Fig 4(f) shows that multilayer islands are observed after annealing at 600°C as well. However, as for Si/Ni(111), the conversion of the faint 2x2 reconstruction to a $(\sqrt{3}x\sqrt{3})R30°$ reconstruction in the LEED patterns in Figs 3 (d) and (f) demonstrates the silicide phase transition from Ni_3Si to Ni_2Si beneath the Gr layer as well.

Finally, increasing the sample temperature above 600°C causes C dissolution in the Ni crystal, as clearly proved by the AES C/Ni sharp signal decrease (Fig. 2) occurring between 600 and 700°C and by the disappearance of the $(\sqrt{3}x\sqrt{3})R30°$ reconstruction in the LEED pattern of the Si/Ni(111) sample, Fig. 3 (h), where only the bulk Ni(111) spots remain visible.

4.3 Role of the epitaxial graphene layer

The high resolution STM images and the relative differentiated images of the Si/Gr/Ni(111) sample after annealing at 450°C and 600°C reported in Fig. 6 confirm the multilayer nature of the silicide islands and reveal that the Gr overlayer covers both the substrate and the multilayer islands terraces. Interestingly, the differentiated STM image in Fig. 6(b) shows areas, highlighted by blue dotted ovals, in which the Gr lattice shows discontinuities, possibly indicating the Gr defects at which Si intercalation occurred, inducing the formation of the multilayer island.

We attribute the formation of multilayer islands, rather than single layer ones observed in the absence of Gr, to a preferential Si intercalation at Gr defects and/or domain boundaries. Indeed, the presence of defects and domain boundaries in epitaxial graphene grown on Ni(111) has been widely discussed in the literature [32-34] and the localized intercalation process at graphene defects

has been reported to occur for many different atomic species deposited on different epitaxial graphene systems [35-37] and, more specifically, for Si on Gr/Ni(111) [18-19].

We observed that graphene greatly affects the Si-Ni reactivity before annealing, impeding the largest part of the deposited Si to react with the Ni substrate at RT. Upon annealing, Si intercalates beneath the graphene layer through defects, determining Si accumulation at specific sample areas. However, the presence of graphene has no effect on the nature of the silicide phases obtained upon annealing, suggesting that the conversion from one silicide phase to the other is a thermodynamically driven process exclusively determined by the annealing temperature increase.

By keeping the annealing temperature below 600°C, this procedure not only produces graphene-protected nickel silicides, exploiting the self-healing characteristics of graphene already occurring at such temperatures [32,38,39], but also opens the path for exploiting the properties of such silicides combined with those of quasi-free-standing graphene. Furthermore, graphene defects may be deliberately induced at specific sample locations to grow silicide islands of the chosen shape or size [40]. Finally, we envisage that, growing graphene on thin Ni(111) films, it would be possible to apply this method to grow nickel silicides structures on the substrate of choice (e.g., Si(100) [41]).

5. Conclusions

In summary, we studied the effect of the presence of a graphene epitaxial layer on the growth of nickel silicides on the Ni(111) substrate. We deposited 1 ML of Si atoms at room temperature and analyzed the chemical and morphological changes occurring upon annealing. We observed that the graphene presence does not influence the chemical nature of the silicide phases obtained at different annealing temperatures, which we identified to be Ni_3Si after annealing at 450°C and Ni_2Si after annealing at 600°C. A further increase of the annealing temperature results in the disappearance of any ordered phase and in a significant Si dissolution in the Ni bulk. Conversely, we found that the presence of the Gr layer has a substantial impact on the morphology of the resulting alloys, causing the formation of large multilayered silicide islands. Indeed, in the absence of a protective Gr layer, the deposited Si atoms can interact with the whole Ni(111) surface area, while in the presence of a graphene layer Si can only intercalate in correspondence of Gr grain boundaries/defects, locally interacting with the Ni substrate and promoting the formation of multilayer islands. Such a result suggests that by governing the graphene defect density and localization one can obtain a controlled growth of ordered nickel silicides on graphene-protected Ni(111), thus opening the path for applications in next generation electronic devices.

Acknowledgements

F. Ronci, S. Colonna and R. Flammini wish to thank G. Emma and M. Ortenzi for technical support. M. Scarselli, M. Salvato, M. De Crescenzi and P. Castrucci would like to acknowledge the European Community for the Horizon 2020 MSCA-RISE Project DisetCom (GA823728). H. Vach would like to acknowledge the HPC centers of IDRIS (Grant A0120900642) and CERMM for computational resources.

References

[1] C. Lavoie, F.M. d'Heurle, C. Detavernier, C. Cabral, Towards implementation of a nickel silicide process for CMOS technologies, Microelectron Eng, 70 (2003) 144-157.
[2] L.F. Dong, J. Bush, V. Chirayos, R. Solanki, J. Jiao, Y. Ono, J.F. Conley, B.D. Ulrich, Dielectrophoretically controlled fabrication of single-crystal nickel silicide nanowire interconnects, Nano Lett, 5 (2005) 2112-2115.
[3] W.M. Weber, L. Geelhaar, A.P. Graham, E. Unger, G.S. Duesberg, M. Liebau, W. Pamler, C. Cheze, H. Riechert, P. Lugli, F. Kreupl, Silicon-nanowire transistors with intruded nickel-silicide contacts, Nano Lett, 6 (2006) 2660-2666.
[4] J.A. Kittl, A. Lauwers, A. Veloso, T. Hoffmann, S. Kubicek, M. Niwa, M.J.H. van Dal, M.A. Pawlak, S. Brus, C. Demeurisse, C. Vrancken, P. Absil, S. Biesemans, CMOS integration of dual work function phase-controlled Ni fully silicided gates (NMOS : NiSi, PMOS : Ni2Si, and Ni31Si12) on HfSiON, IEEE Electr Device Letters, 27 (2006) 966-968.
[5] J.A. Kittl, K. Opsomer, C. Torregiani, C. Demeurisse, S. Mertens, D.P. Brunco, M.J.H. Van Dal, A. Lauwers, Silicides and germanides for nano-CMOS applications, Mater Sci Eng B-Adv, 154 (2008) 144-154.
[6] K.T. Butler, J.H. Harding, A computational investigation of nickel (silicides) as potential contact layers for silicon photovoltaic cells, J Phys-Condens Mat, 25 (2013) 395003.
[7] M. Bhaskaran, S. Sriram, L.W. Sim, Nickel silicide thin films as masking and structural layers for silicon bulk micro-machining by potassium hydroxide wet etching, J Micromech Microeng, 18 (2008) 095002.
[8] P. Nash, A. Nash, The Ni−Si (Nickel-Silicon) system, Bullettin of Alloy Phase Diagrams, 8 (1987) 6–14.
[9] H. Von Känel, Growth and Characterization of Epitaxial Ni and Co Silicide, Mater Sci Rep, 8 (1992) 193-269.
[10] L. Gregoratti, S. Gunther, J. Kovac, M. Marsi, R.J. Phaneuf, M. Kiskinova, Ni/Si(111) system: Formation and evolution of two- and three-dimensional phases studied by spectromicroscopy, Phys. Rev. B, 59 (1999) 2018-2024.
[11] P.A. Bennett, M.Y. Lee, S.A. Parikh, K. Wurm, R.J. Phaneuf, Surface Phase-Transformations in the Ni/Si(111) System Observed in Real-Time Using Low-Energy-Electron Microscopy, J Vac Sci Technol A, 13 (1995) 1728-1732.
[12] C.H.T. Chang, P.C. Jiang, Y.T. Chow, H.L. Hsiao, W.B. Su, J.S. Tsay, Enhancing silicide formation in Ni/Si(111) by Ag-Si particles at the interface, Sci Rep, 9 (2019) 8835.

[13] G. Kinoda, K. Ogawa, Scanning tunneling microscope studies on twinned atomic structures of root 19 x root 19 surface reconstruction in the Ni/Si(111) system, Surf Sci, 461 (2000) 67-77.
[14] B. Lalmi, C. Girardeaux, A. Portavoce, C. Ottaviani, B. Aufray, J. Bernardini, Formation and stability of a two-dimensional nickel silicide on Ni(111): An Auger, LEED, STM, and high-resolution photoemission study, Phys Rev B, 85 (2012) 245306.
[15] M.S. Rahman, T. Nakagawa, S. Mizuno, Structure determination of the ordered (root 3 x root 3)R30 degrees phase of Ni2Si and Ni2Ge surface alloys on Ni(111) via low-energy electron diffraction, Surf Sci, 642 (2015) 1-5.
[16] T. Fukuda, I. Kishida, K. Umezawa, Formation of two-dimensional silicide on Ni(100) surface, Jpn J Appl Phys, 59 (2020) 065501.
[17] M.S. Rahman, M.A. Islam, B.B. Saha, T. Nakagawa, S. Mizuno, Structure determination of the ordered (2 x 1) phase of NiSi surface alloy on Ni(111) using low-energy electron diffraction, Jpn J Appl Phys, 54 (2015) 125701.
[18] O. Vilkov, A. Fedorov, D. Usachov, L.V. Yashina, A.V. Generalov, K. Borygina, N.I. Verbitskiy, A. Gruneis, D.V. Vyalikh, Controlled assembly of graphene-capped nickel, cobalt and iron silicides, Sci. Rep., 3 (2013) 2168.
[19] F. Ronci, S. Colonna, R. Flammini, M. De Crescenzi, M. Scarselli, M. Salvato, I. Berbezier, F. Jardali, C. Lechner, P. Pochet, H. Vach, P. Castrucci, High graphene permeability for room temperature silicon deposition: The role of defects, Carbon, 158 (2020) 631-641.
[20] U. DelPennino, P. Sassaroli, S. Valeri, C.M. Bertoni, O. Bisi, C. Calandra, Effects of chemical environment in the lineshape of silicon L2, 3VV Auger spectra of nickel silicides, Journal of Physics C: Solid State Physics, 16 (1983) 6309-6319.
[21] R. Larciprete, S. Colonna, F. Ronci, R. Flammini, P. Lacovig, N. Apostol, A. Politano, P. Feulner, D. Menzel and S. Lizzit, Self-Assembly of Graphene Nanoblisters Sealed to a Bare Metal Surface, Nano Lett., 16 (2016) 1808.
[22] T. Iwasaki, H.J. Park, M. Konuma, D.S. Lee, J.H. Smet, U. Starke, Long-range ordered single-crystal graphene on high-quality heteroepitaxial Ni thin films grown on MgO(111), Nano Lett. 11 (2011) 79-84
[23] F. Jona, Reactions of silicon with surfaces of close-packed metals. II. Silicon on nickel, J. Appl. Phys., 44 (1973) 351-356.
[24] G. Ottaviani, Review of binary alloy formation by thin film interactions, Journal of Vacuum Science & Technology 16 (1979) 1112.
[25] Y. Cao, L. Nyborg, U. Jelvestam, XPS calibration study of thin-film nickel silicides, Surf Interface Anal, 41 (2009) 471-483.
[26] S. Gaudet, P. Desjardins, C. Lavoie, The thermally-induced reaction of thin Ni films with Si: Effect of the substrate orientation, J Appl Phys, 110 (2011) 113524.
[27] C.J. Tsai, K.H. Yu, Stress evolution during isochronal annealing of Ni/Si system, Thin Solid Films, 350 (1999) 91-95.
[28] K. Kanematsu, Stability of the Crystal Structure of $(Fe, V)_3M$ and $(Fe, Ni)_3M$ (M= Si, Ge, Sn) and its Analysis Based on Rigid Band Model, Transactions of the Japan Institute of Metals, 27 (1986) 225-232.
[29] S. Bhan, H. Kudielka, Ordered bcc-phases at high temperatures in alloys of transition metals and B-subgroup elements, Zeitschrift fuer Metallkunde, 69 (1978) 333-336
[30] K. Toman, The structure of Ni2 Si, Acta Crystallographica 5 (1952) 329-331.
[31] M. Ellner, M.K. Bhargava, S. Heinrich, K. Schubert, Einige strukturelle Untersuchungen in der Mischung $NiSi_N$, Journal of the Less-Common Metals, 66 (1979) 163-173.

[32] P. Jacobson, B. Stöger, A. Garhofer, G. S. Parkinson, M. Schmid, R. Caudillo, F. Mittendorfer, J. Redinger, and U. Diebold, Disorder and Defect Healing in Graphene on Ni(111), J. Phys. Chem.Lett., 3 (2012) 136−139.
[33] A. Dahal and M. Batzill, Graphene–nickel interfaces: a review, Nanoscale, 6 (2014) 2548–2562.
[34] F. Bianchini, L. L. Patera, M. Peressi, C. Africh, and G. Comelli, Atomic Scale Identification of Coexisting Graphene Structures on Ni(111), J. Phys. Chem. Lett., 5 (2014) 467−473.
[35] A. Ya. Tontegode and E. V. Rut'kov, Intercalation by atoms of a two-dimensional graphite film on a metal , Phys.-Usp. 36 (1993) 1053.
[36] G. S. Grebenyuk, O. Yu. Vilkov, A. G. Rybkin, M. V. Gomoyunova, B. V. Senkovskiy, D. Yu. Usachov, D. V. Vyalikh, S. L. Molodtsov, I. I. Pronin, Intercalation synthesis of graphene-capped iron silicide atop Ni(111): Evolution of electronic structure and ferromagnetic ordering, Applied Surface Science 392 (2017) 715–72.
[37] N. Briggs, Z. M. Gebeyehu, A. Vera, T. Zhao, K. Wang, A. De La Fuente Duran, B. Bersch, T. Bowen, K. L. Knappenberger Jr., and J. A. Robinson, Epitaxial graphene/silicon carbide intercalation: a minireview on graphene modulation and unique 2D materials, Nanoscale, 11 (2019) 15440.
[38] J. Chen, T Shi, T. Cai, T. Xu, L. Sun, X. Wu and D. Yu, Self-healing of defected graphene, Appl. Phys. Lett. 102, 103107 (2013).
[39] G. Li, P. Xiao, S. Hou, Y. Huang, Graphene based self-healing materials, Carbon 146 (2019), 371-387.
[40] C.-L. Wu, H.-T. Lin, H.-A. Chen, S.-Y. Lin, M.-H. Shin, C.-W. Pao, Defect formation and modulation during patterning supported graphene sheets using focused ion beams, Materials Today Communications 17, (2018) 60-68.
[41] W. Kreuzpaintner, M. Störmer, D. Lott, D. Solina, and A. Schreyer, Epitaxial growth of nickel on Si(100) by dc magnetron sputtering, J. Appl. Phys. 104 (2008) 114302.

CRediT author statement

Fabio Ronci: Conceptualization, Methodology, Validation, Formal analysis, Investigation, Resources, Writing - Original Draft, Writing - Review & Editing, Visualization, Supervision, Project administration
Stefano Colonna: Conceptualization, Methodology, Validation, Investigation, Writing - Original Draft, Writing - Review & Editing
Roberto Flammini: Methodology, Validation, Investigation, Writing - Review & Editing
Maurizio De Crescenzi: Writing - Review & Editing
Manuela Scarselli: Writing - Review & Editing
Matteo Salvato: Writing - Review & Editing
Isabelle Berbezier: Writing - Review & Editing
Holger Vach: Writing - Review & Editing
Paola Castrucci: Conceptualization, Resources, Writing - Original Draft, Writing - Review & Editing, Supervision

Declaration of interests

☐The authors declare that they have no known competing financial interests or personal relationships that could have appeared to influence the work reported in this paper.

☒The authors declare the following financial interests/personal relationships which may be considered as potential competing interests:

M. Scarselli, M. Salvato, M. De Crescenzi, P. Castrucci reports financial support was provided by European Commission Marie Sklodowska-Curie Actions. H. Vach reports equipment, drugs, or supplies was provided by Compute Canada. H. Vach reports equipment, drugs, or supplies was provided by Centre National de la Recherche Scientifique.

Graphical abstract

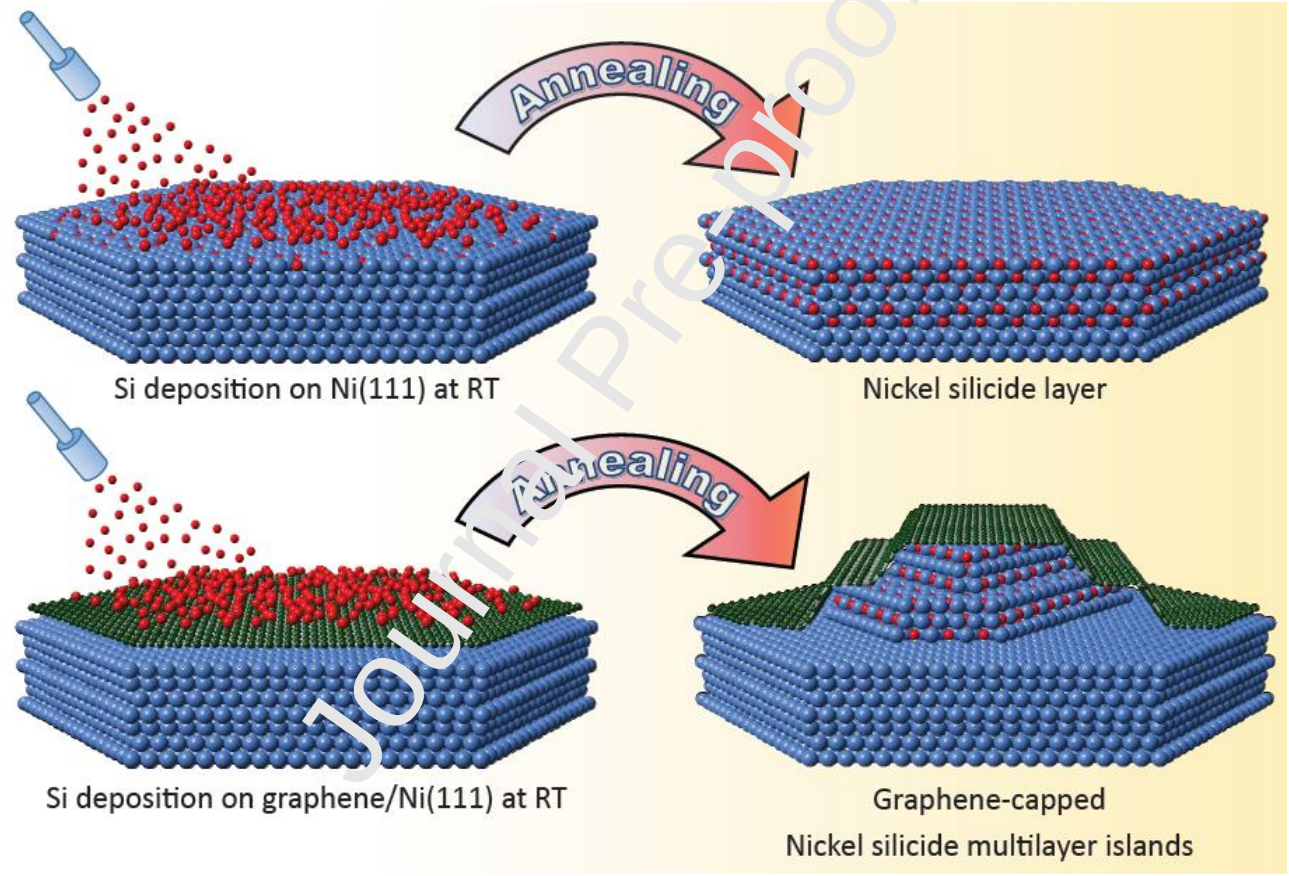

Highlights

- Silicon was deposited at room temperature on Ni(111) and graphene-covered Ni(111)
- The formation of nickel silicides upon annealing was studied on the two substrates
- Ni_3Si and Ni_2Si are formed on both substrates at 450°C and at 600°C, respectively
- With graphene, multilayer silicide islands are formed only at graphene defects
- Graphene self-healing consents graphene-protected Ni_xSi growth on Ni(111)

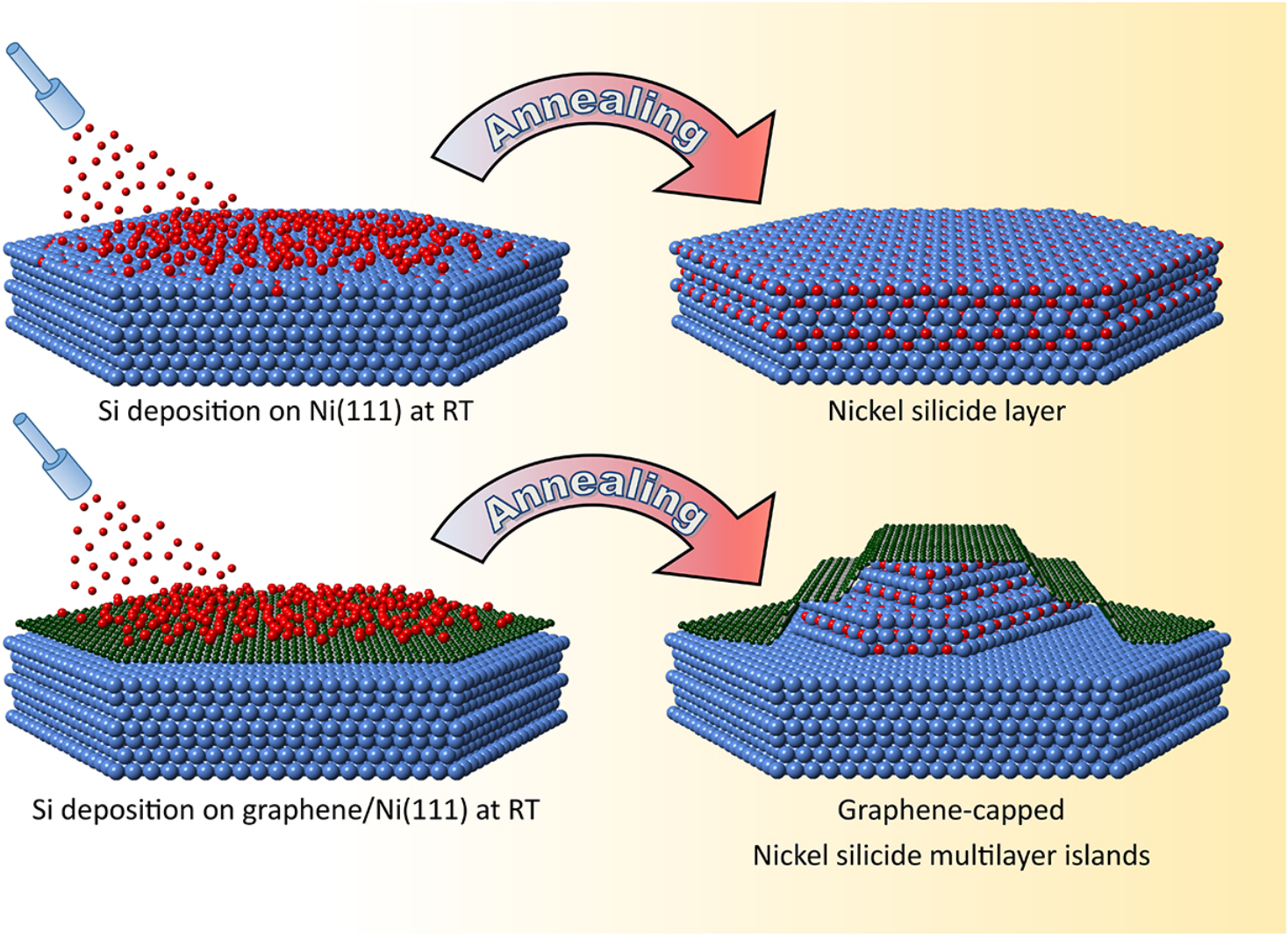

Graphics Abstract

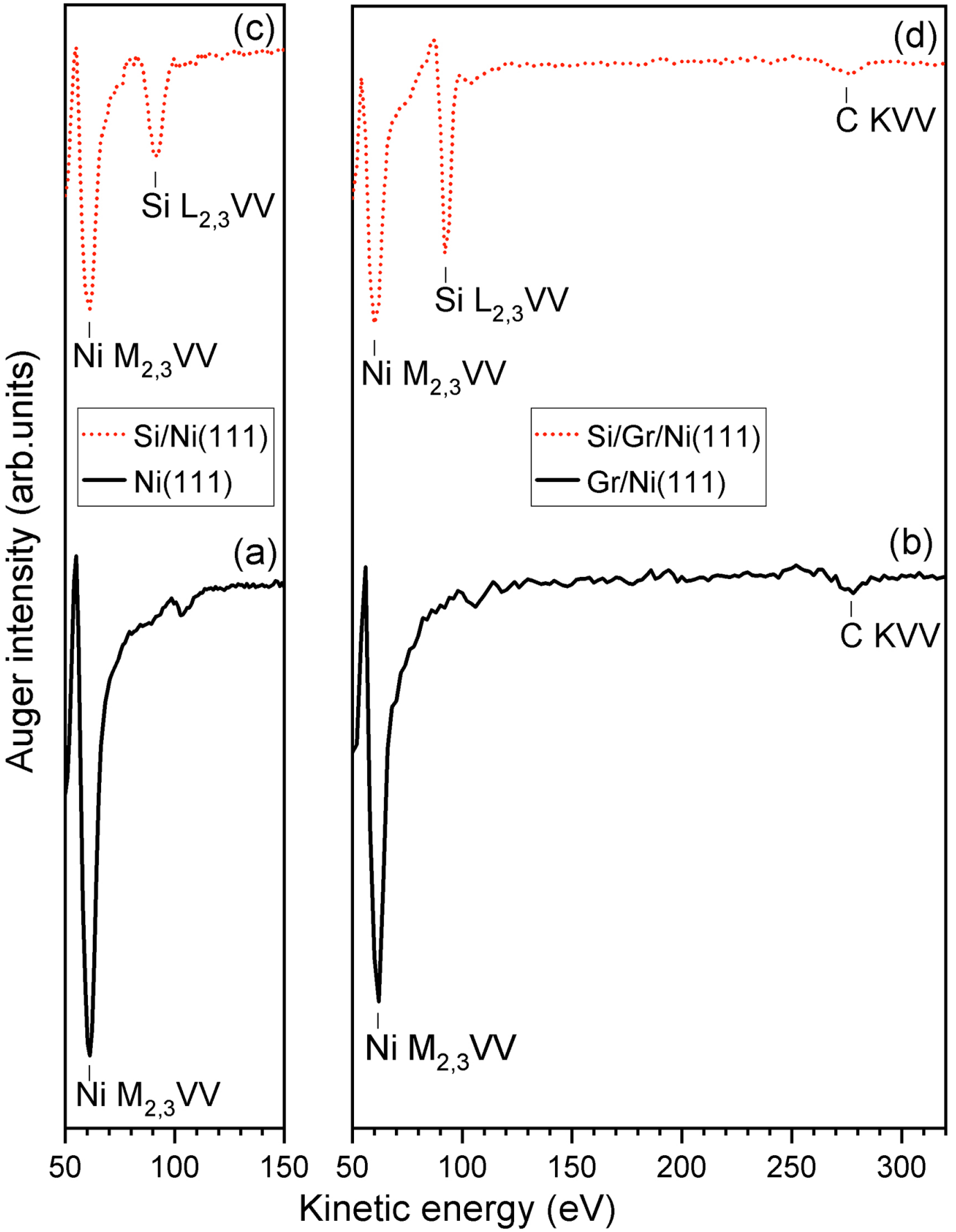
(c)
Si $L_{2,3}VV$
Ni $M_{2,3}VV$
Si/Ni(111)
Ni(111)
(a)
Ni $M_{2,3}VV$
(d)
C KVV
Si $L_{2,3}VV$
Ni $M_{2,3}VV$
Si/Gr/Ni(111)
Gr/Ni(111)
(b)
C KVV
Ni $M_{2,3}VV$
Auger intensity (arb.units)
50
100
150
50
100
150
200
250
300
Kinetic energy (eV)

Figure 1

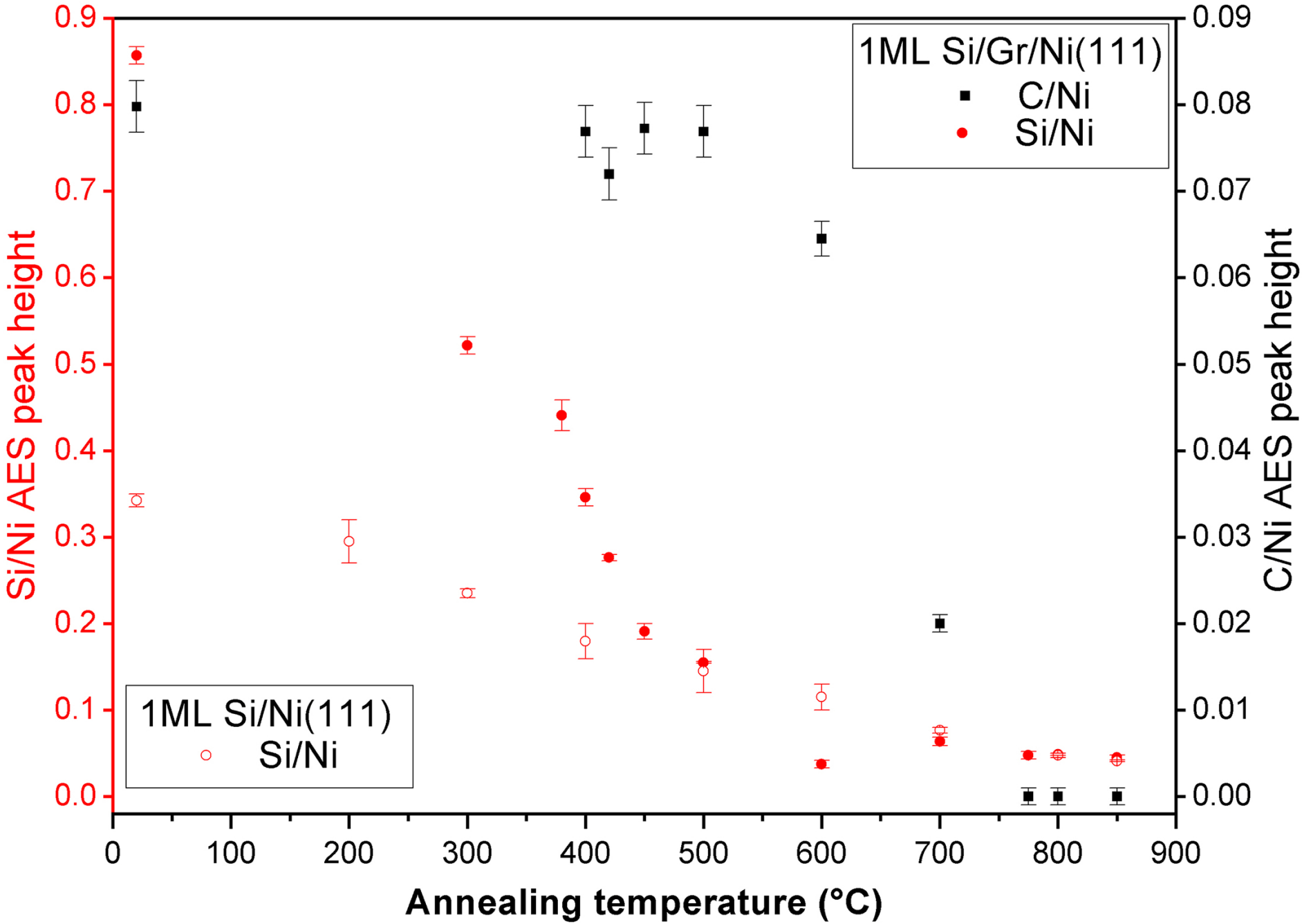
1ML Si/Gr/Ni(111)
C/Ni
Si/Ni
1ML Si/Ni(111)
Si/Ni
Si/Ni AES peak height
C/Ni AES peak height
Annealing temperature (°C)
0.0
0.1
0.2
0.3
0.4
0.5
0.6
0.7
0.8
0.9
0.00
0.01
0.02
0.03
0.04
0.05
0.06
0.07
0.08
0.09
0
100
200
300
400
500
600
700
800
900

Figure 2

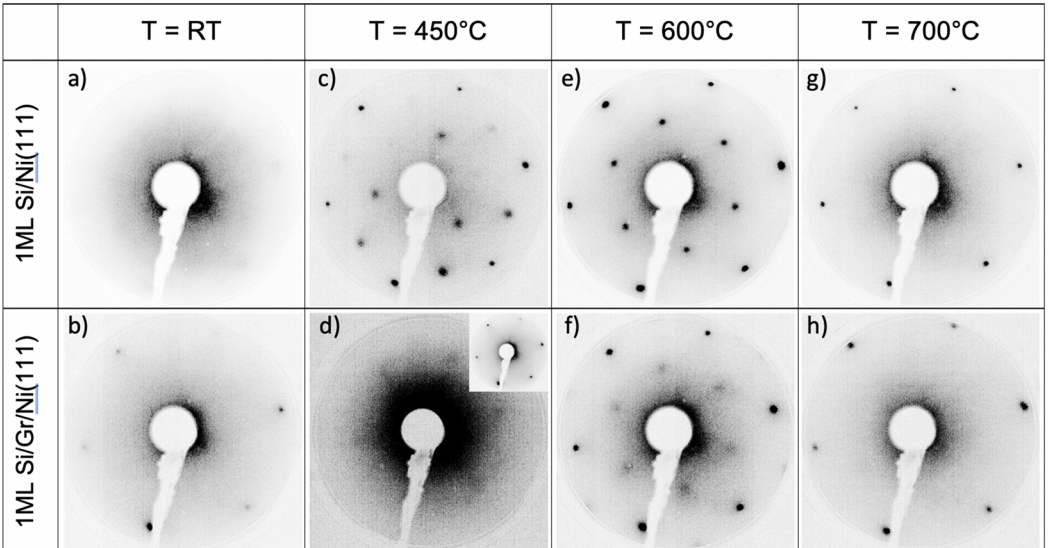

Figure 3

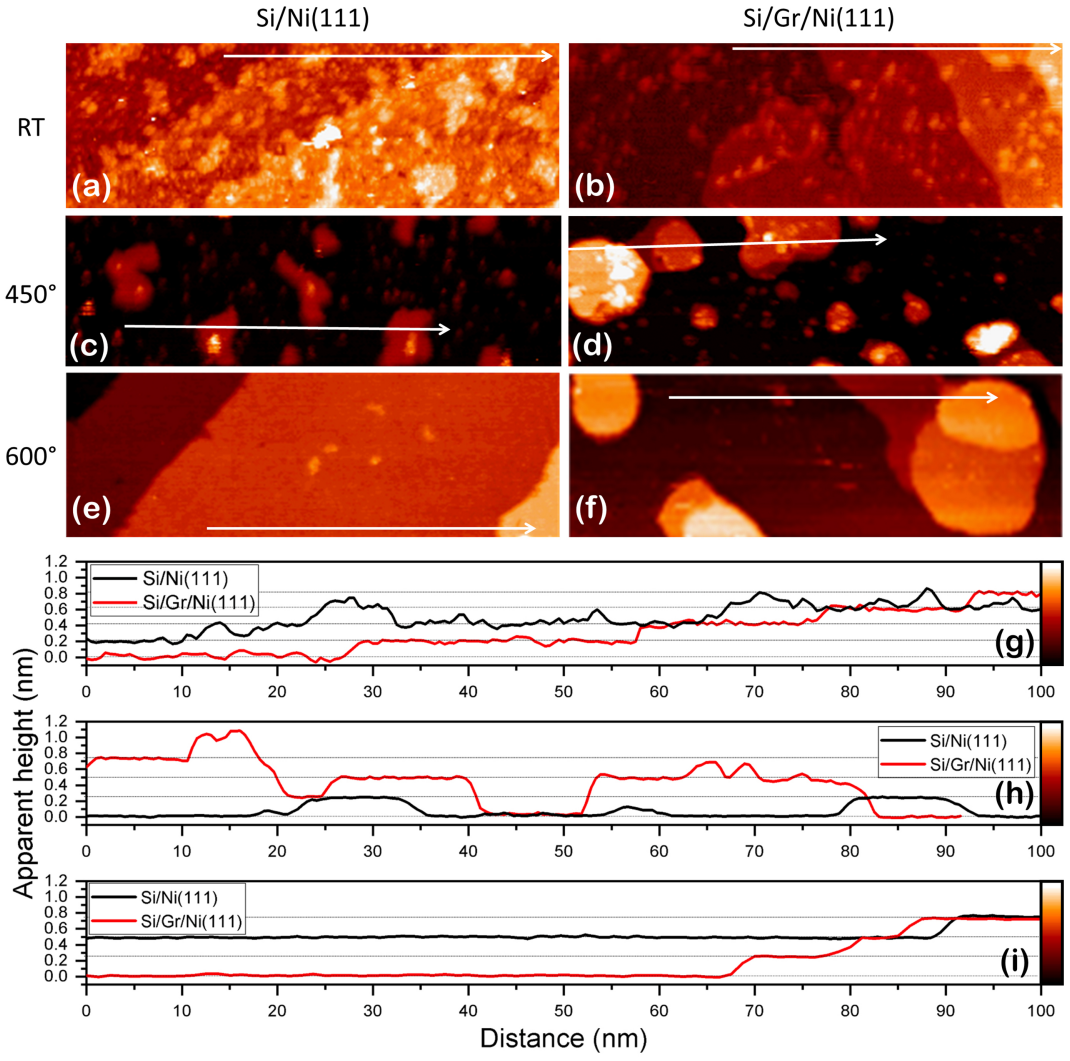
Si/Ni(111)
Si/Gr/Ni(111)
RT
450°
600°
(a)
(b)
(c)
(d)
(e)
(f)
Si/Ni(111)
Si/Gr/Ni(111)
(g)
(h)
(i)
Apparent height (nm)
Distance (nm)

Figure 4

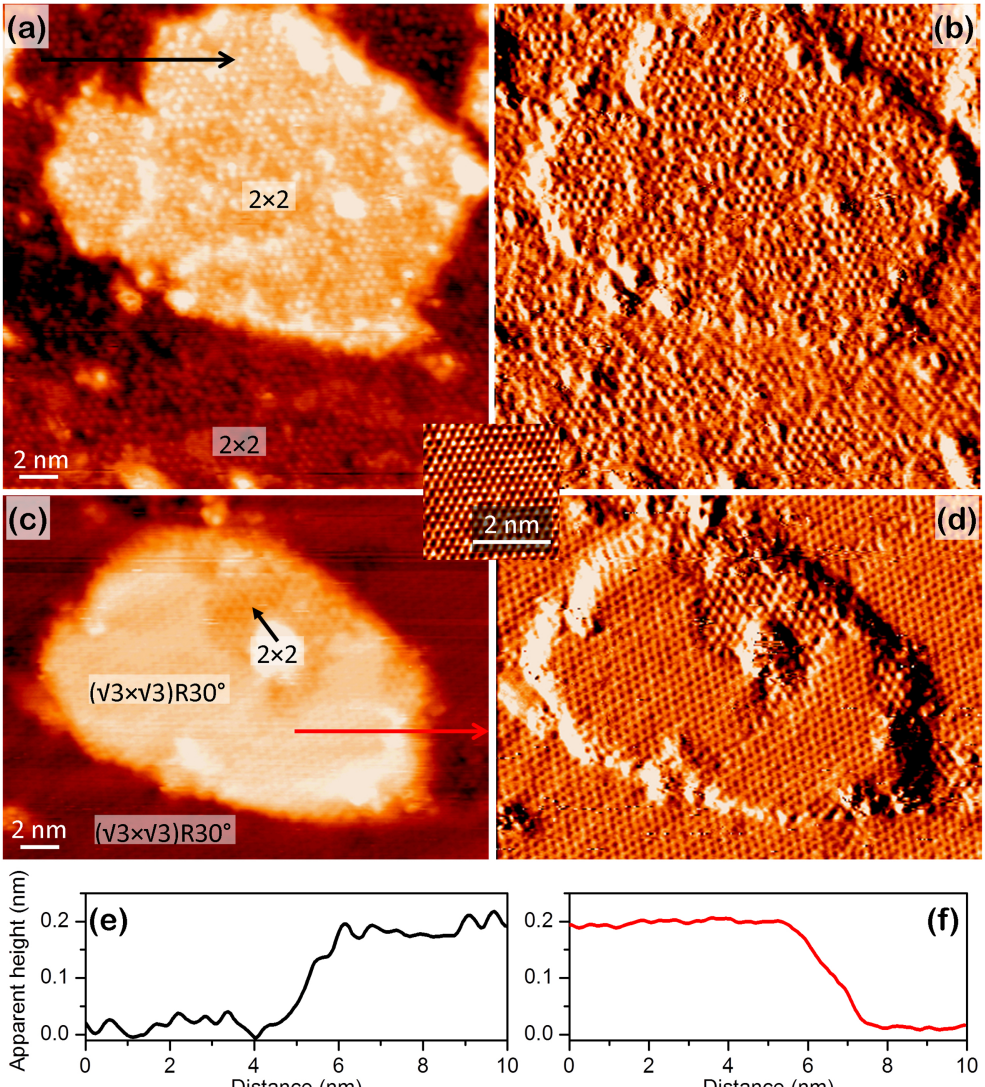
(a)
2×2
2×2
2 nm
(b)
2 nm
(c)
2×2
(√3×√3)R30°
2 nm
(√3×√3)R30°
(d)
(e)
Apparent height (nm)
0.2
0.1
0.0
0
2
4
6
8
10
Distance (nm)
(f)
0.2
0.1
0.0
0
2
4
6
8
10
Distance (nm)

Figure 5

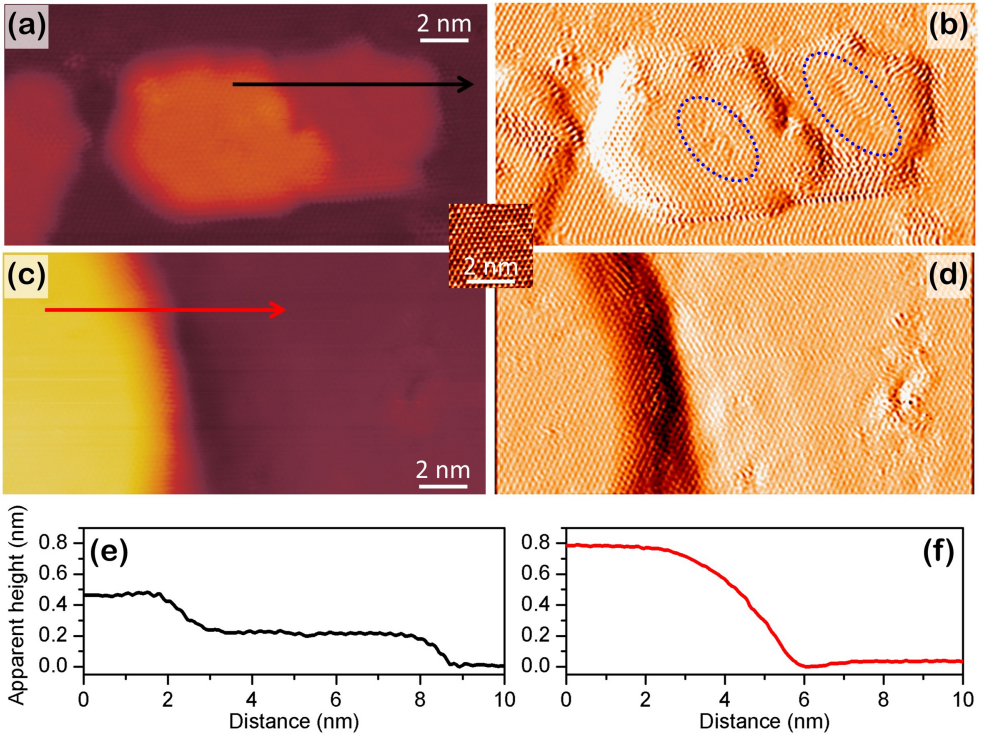
(a)
2 nm
(b)
2 nm
(c)
2 nm
(d)
(e)
(f)
Apparent height (nm)
0.0
0.2
0.4
0.6
0.8
0
2
4
6
8
10
Distance (nm)
Distance (nm)

Figure 6

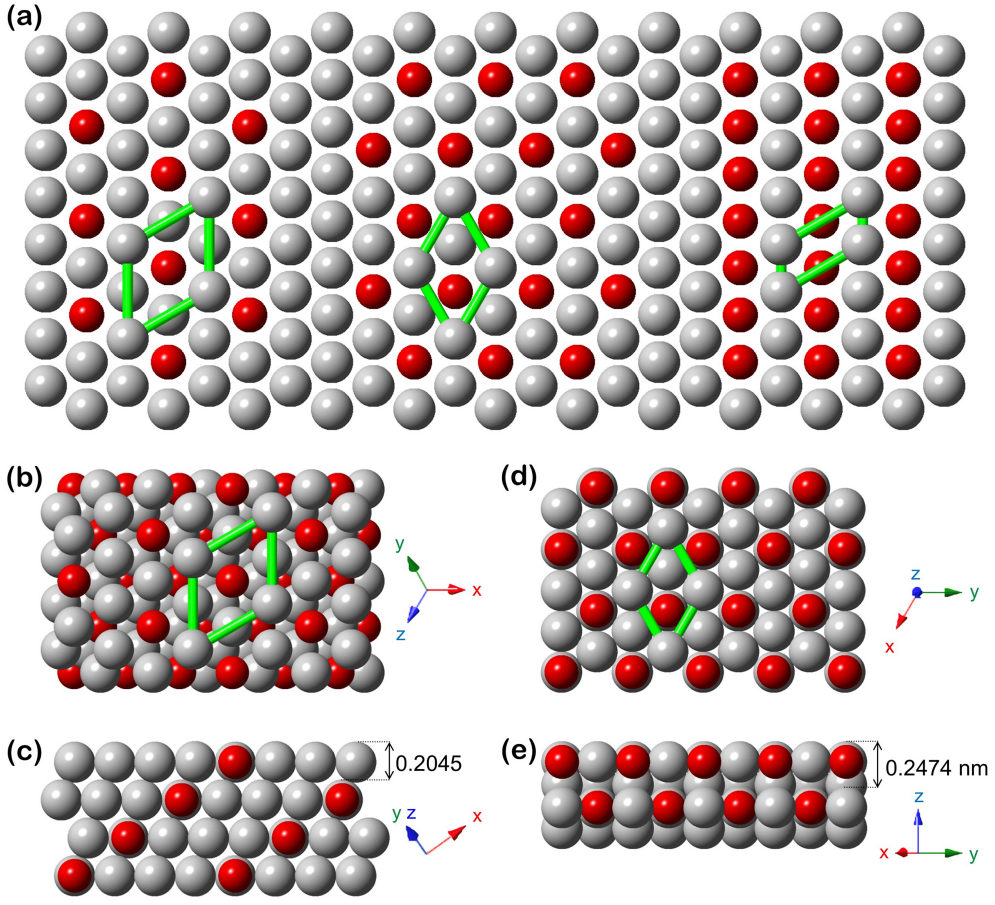

Figure 7